Extracellular Vesicles from hiPSC-derived NSCs Protect Human Neurons against Aβ-42 Oligomers Induced Neurodegeneration, Mitochondrial Dysfunction and Tau Phosphorylation

Shama Rao, Leelavathi N Madhu, Roshni Sara Babu, Advaidhaa Nagarajan, Raghavendra Upadhya, Esha Narvekar and Ashok K Shetty*

Institute for Regenerative Medicine, Department of Cell Biology and Genetics, Texas A&M University Health Science Center School of Medicine, College Station, Texas, USA

Keywords: Aβ-42 oligomers, Alzheimer's disease, Apoptosis, Autophagy, Mitochondrial hyperactivation, Neural stem cells, Neurotoxicity, Oxidative stress, and Stem cell-derived extracellular vesicles.

***Address for Correspondence:**

Ashok K. Shetty, Ph.D.
University Distinguished Professor
Associate Director and Professor
Institute for Regenerative Medicine, Department of Cell Biology and Genetics,
Texas A&M University School of Medicine,
1114 TAMU, 206 Olsen Boulevard
College Station, TX 77843
E-mail: ash.shetty@tamu.edu

Abstract

Background: One of the hallmarks of Alzheimer's disease (AD) is the buildup of amyloid beta-42 (Aβ-42) in the brain, which leads to various adverse effects. Therefore, therapeutic interventions proficient in reducing Aβ-42-induced toxicity in AD are of great interest. One promising approach is to use extracellular vesicles from human induced pluripotent stem cell-derived neural stem cells (hiPSC-NSC-EVs) because they carry multiple therapeutic miRNAs and proteins capable of protecting neurons against Aβ-42-induced pathological changes. Therefore, this *in vitro* study investigated the proficiency of hiPSC-NSC-EVs to protect human neurons derived from two distinct hiPSC lines from Aβ-42o-induced neurodegeneration.

Methods: We isolated hiPSC-NSC-EVs using chromatographic methods and characterized their size, ultrastructure, expression of EV-specific markers and proficiency in getting incorporated into mature human neurons. Next, mature human neurons differentiated from two different hiPSC lines were exposed to 1 µM Aβ-42 oligomers (Aβ-42o) alone or with varying concentrations of hiPSC-NSC-EVs. The protective effects of hiPSC-NSC-EVs against Aβ-42o-induced neurodegeneration, increased oxidative stress, mitochondrial dysfunction, impaired autophagy, and tau phosphorylation were ascertained using multiple measures and one-way ANOVA with Newman-Keuls multiple comparisons post hoc tests.

Results: Significant neurodegeneration was observed when human neurons were exposed to Aβ-42o alone. Notably, neurodegeneration was associated with elevated levels of oxidative stress markers malondialdehyde (MDA) and protein carbonyls (PCs), increased expression of proapoptotic Bax and Bad genes and proteins, reduced expression of the antiapoptotic gene and protein Bcl-2, increased expression of genes encoding mitochondrial complex proteins, decreased expression of autophagy-related proteins Beclin-1 and microtubule-associated protein 1 light chain 3B, and increased phosphorylation of tau. However, the addition of an optimal dose of hiPSC-NSC-EVs (6×10^9 EVs) to human neuronal cultures exposed to Aβ-42o significantly reduced the extent of neurodegeneration, along with diminished levels of MDA and PCs, normalized expressions of Bax, Bad, and Bcl-2, and genes linked to mitochondrial complex proteins, and reduced tau phosphorylation.

Conclusions: The findings demonstrate that an optimal dose of hiPSC-NSC-EVs could significantly decrease the degeneration of human neurons induced by Aβ-42o. The results also support further research into the effectiveness of hiPSC-NSC-EVs in AD, particularly their proficiency in preserving neurons and slowing disease progression.

Introduction

Alzheimer's disease (AD) is the fifth leading cause of death, impacting ~47 million people globally and 7 million people in the United States [1]. It is projected that by 2050, AD-related dementia will affect ~13 million individuals in the United States [2]. The most prominent pathological features of AD are the accumulation of amyloid plaques in the extracellular space and the neurofibrillary tangles (NFTs) within neurons. These alterations contribute to the progressive loss of synapses, significant chronic neuroinflammation, and eventual neurodegeneration and dementia [3,4]. Amyloid plaques consist of amyloid beta peptide (Aβ), while NFTs contain phosphorylated tau protein [5,6]. The Aβ protein is primarily produced by neurons and, to a lesser extent, by astrocytes in the brain. Additionally, vascular cells and blood cells also generate Aβ [7]. Aβ is created through a series of proteolytic cleavages of amyloid precursor protein (APP) by β- and γ-secretases [8]. After its release, soluble Aβ monomers form dimers, trimers, soluble oligomers, and protofibrils, eventually leading to the formation of fibrils that accumulate in plaques [3]. The main forms of Aβ in the human brain are Aβ1−40 (Aβ-40) and Aβ1−42 (Aβ-42), with Aβ-42 forming aggregates due to being less soluble than Aβ-40 [3,9]. Therefore, Aβ-42 contributes to the pathogenesis of AD and is considered one of the key biomarkers in AD diagnosis [10,11].

While Aβ-42 monomers play roles in neuronal cytoprotective pathways, intracellular signaling, and synaptic functions [12,13], Aβ-42 oligomers (Aβ-42o) can induce neurotoxicity. For example, injection of Aβ-42o into rodent hippocampus can diminish long-term potentiation (LTP), enhance long-term depression (LTD), and cause synapse loss [14–16]. *In vitro* studies using Aβ-42o have reported similar effects on LTP in brain slices [17] and neurotoxicity in rat cortical neurons [18]. Therefore, Aβ-42o pathophysiology seems to be an initial pathological event in AD that triggers subsequent molecular pathways, including tau misfolding, tau buildup in NFTs, and tau-mediated toxicity [11,19–22]. The accumulation of Aβ-42o in the brain leads to various harmful effects. For instance, Aβ-42o can induce increased oxidative stress by inserting into the lipid bilayer, serving as a source of reactive oxygen species (ROS), and initiating lipid peroxidation [23–25]. Additionally, Aβ-42o can localize to mitochondrial membranes, reduce mitochondrial membrane potential, block the transport of nuclear-encoded mitochondrial proteins to mitochondria, disrupt the electron transport chain, increase ROS production, and cause mitochondrial damage [26]. Exposure of neurons to Aβ-42o can also reduce mitochondrial superoxide dismutase 2 and mitochondrial cytochrome C protein [27]. Furthermore,

mitochondrial-specific accumulation of Aβ-42o induces mitochondrial dysfunction leading to apoptotic cell death [28]. Apoptotic cell death in response to Aβ-42o exposure involves altered expression of pro- and anti-apoptotic proteins [29]. Furthermore, Aβ-42o exposure to neurons can significantly increase the phosphorylation of tau protein by activating tau kinases, mitogen-activated protein kinase, and glycogen synthase kinase-3 beta [30,31]. Therefore, there is a keen interest in therapeutic interventions aimed at reducing Aβ-42o-induced toxicity in AD.

One potential approach for safeguarding neurons from Aβ-42o induced toxicity in AD is using extracellular vesicles (EVs) released from stem cells, as these EVs contain various therapeutic miRNAs and proteins that can protect neurons [32–35]. However, no previous studies have tested the effectiveness of neural stem cell (NSC)-derived EVs in amyloid toxicity models. Recent studies in our laboratory have demonstrated that EVs released by human induced pluripotent stem cell (hiPSC)-derived NSCs (hiPSC-NSC-EVs) are enriched with miRNAs and proteins that can mediate antioxidant, antiapoptotic, anti-inflammatory, and neurogenic effects [36–38]. Furthermore, hiPSC-NSC-EVs contain specific miRNAs (miRNA-103a, miRNA-21-5p) and proteins (pentraxin-3) that can promote neuroprotection, including through antiapoptotic mechanisms [39–42]. Additional miRNA (miRNA-181) and protein (hemopexin) enriched in hiPSC-NSC-EVs can maintain mitochondrial function and homeostasis [43] and reduce ROS toxicity [36,44]. Moreover, the absence of tumorigenic and immunogenic properties, combined with the capacity to efficiently penetrate the entire brain and integrate into neurons following intranasal administrations [36,45] positions hiPSC-NSC-EVs as a compelling biologic for conferring neuroprotection in neurodegenerative disorders. Therefore, the current *in vitro* study examined whether hiPSC-NSC-EVs could protect human neurons derived from two different hiPSC lines against Aβ-42o-induced neurodegeneration. The results provide novel evidence that an optimal dosage of hiPSC-NSC-EVs could markedly avert Aβ-42o-induced neurodegeneration through the reduction of oxidative stress, attenuation of mitochondrial hyperactivation, modulation of pro-apoptotic and antiapoptotic gene and protein expression, regulation of autophagy, and mitigation of tau phosphorylation.

Materials and Methods

Differentiation of hiPSC-NSCs into neurons.

The mature human neurons used in these studies were freshly differentiated from NSCs generated from two hiPSC lines: one from Wisconsin International Stem Cell Bank (IMR90-4) and the other from the National Institutes of Health (NIH; LiPSC-GR1.1, Research grade). The hiPSCs were first transformed into NSCs using a directed differentiation protocol, as described in our previous studies [36,37]. The NSCs were then seeded onto 24-well plates that were coated with 0.1 mg/ml of poly-D-lysine (Sigma Aldrich, St. Louis, MO, USA) and 10 µg/ml laminin (Corning Inc., Corning, NY, USA) at a density of 15,000 cells/cm^2 using neuronal differentiation media. The media comprised Neurobasal (Thermo Fisher Scientific), Glutamax (Thermo Fisher Scientific), and B27 supplement with retinoic acid (Thermo Fisher Scientific) at a ratio 98:1:1 for 30 days to enable complete differentiation into neurons. The neuronal differentiation was confirmed through immunofluorescence staining using antibodies against microtubule-associated protein-1 (rabbit anti-MAP2; Millipore, Burlington, Massachusetts, USA) and neuron-specific nuclear antigen (rabbit anti-NeuN; Millipore).

Isolation hiPSC-NSC-EVs via chromatographic methods.

After reaching 80% confluency, passage 10 hiPSC-NSCs were dislodged using TrypLE^{TM} Express enzyme (Thermo Fisher Scientific, Waltham, MA, USA), washed with NSC expansion medium containing equal volumes of Neurobasal media and DMEM/F-12 (Thermo Fisher Scientific), Neural Induction supplement (1% of media, Thermo Fisher Scientific) and penicillin-streptomycin (1000 units, ThermoFischer Scientific), and then seeded at 1000 cells/cm^2 onto T300 tissue culture flasks (VWR, Radnor, Pennsylvania, USA) containing fresh NSC expansion medium. The NSCs were maintained for 7 days, and spent media were harvested twice on day 4 and 7. The EVs were isolated using anion-exchange chromatography (AEC) followed by size exclusion chromatography (SEC). The SEC fractions containing a higher number of EVs with lower protein content were combined, concentrated, and stored at −20°C for future use.

Characterization of hiPSC-NSC-EVs for EV-specific marker expression.

We used nanoparticle tracking analysis to determine the concentration and size of EVs, as outlined in our previous studies [36,37]. We assessed the presence of EV-specific tetraspanin markers CD63 and CD81, intra-EV marker protein ALIX, and a non-EV marker cytochrome C using western blotting. In brief, we mixed 25 x 10^9 EVs with 100 µl of a mammalian protein extractor reagent (Thermo Fischer Scientific), lysed it as previously described [46], and the total protein concentration was determined using the Pierce BCA protein assay kit (ThermoFisher Scientific). Next, we loaded and separated 40 µg of protein using 4-12% NuPAGE Bis-Tris Gels (ThermoFisher Scientific). The proteins were then transferred onto nitrocellulose membranes using ThermoFisher Scientific's iBlot2 gel transfer technology. We processed the membrane for protein detection using antibodies against CD63 (1:1000; BD Biosciences, San Jose, California, USA), CD81 (1:1000; BD Biosciences), and ALIX (1:1000; Santa Cruz Biotechnology, Santa Cruz, CA, USA). The s signal was detected using ibright 1500 (Thermo Fischer Scientific) and an ECL kit (Thermo Fischer Scientific). In addition, we examined the expression of cytochrome C to check for contamination of EV preparations with deep cellular proteins compared to the hNSC lysate [36].

Visualization of the morphology of hiPSC-NSC-EVs through transmission electron microscopy.

We used transmission electron microscopy (TEM) to examine the ultrastructure of hiPSC-NSC-EVs, following the methods outlined in our previous studies [36,47]. To do this, we placed 5 µl (~1.5 x 10^9 EVs) of the EV suspension, diluted in PBS, on 300 mesh carbon-coated copper grids (Electron Microscopy Sciences, Hatfield, PA, USA) at room temperature. After five minutes, we blotted the excess liquid from the grids with filter paper and rinsed them twice with distilled water. We then stained the grids by continuously dripping a 150 µl solution of 0.5% uranyl acetate at a 45° inclination. After removing the excess liquid, we air-dried the grids at room temperature for 10 minutes. The images were captured using an FEI Morgagni 268 transmission electron microscope with a MegaView III CCD camera. Lastly, we computed the diameters of hNSC-EVs using the "Analyze" tool in the ImageJ software, averaging the measured diameters along four axes (x, y, x + 45°, y + 45°).

Evaluation of the neuroprotective effects of hiPSC-NSC-EVs on neurons exposed to Aβ-42o.

First, 30-day-old human neuronal cultures were exposed to various doses of Aβ-42o (Sigma-Aldrich, St. Louis, Missouri, USA), ranging from 0.1 µM to 5 µM, for 24 hours to determine the dose-

dependent cytotoxicity using the MTT assay. For subsequent studies, 30-day-old human neuronal cultures were exposed to 1 µM Aβ-42o and were treated concurrently with hiPSC-NSC-EVs at three different concentrations (1.5, 3.0, or 6 x10^9, 3 (n=3 independent cultures/group). Additionally, separate sets of control sister cultures with or without Aβ-42o exposure were maintained (n=3/group). Following a 24-hour incubation period, the neuronal cultures were utilized for various assays.

Visualization of the interaction of cultured human neurons exposed to Aβ-42o with hiPSC-NSC-EVs.

The hiPSC-NSC-EVs were labeled with the PKH26 dye using the PKH26 Red Fluorescent Cell Linker Kit for general cell membrane labeling (Sigma-Aldrich). Approximately 30 x 10^9 EVs were mixed with 100 µl of PBS without calcium and magnesium, followed by the addition of 900 µl of diluent C. Then, 4 µl of PKH26 dye was added to the mixture to achieve a final concentration of 8 µM (dye solution). After 10 minutes of incubation in the dark, the 1 ml preparation was diluted to a final volume of 5 ml using PBS without calcium and magnesium, then centrifuged using filtration columns (100 kDa). This washing step was repeated four times to remove the excess dye from the EV preparation. These EVs (1X10^9) were introduced to mature human neuronal cultures exposed to 1 µM Aβ-42o, and the cultures were fixed after 4 hours of incubation. The cultures were then processed for MAP-2 immunofluorescence to observe EVs contacting neurons, including their internalization by neurons. The interactions were photographed using a fluorescent microscope.

Cytotoxicity measurement by MTT assay.

After incubating human neuronal cultures with Aβ-42o or Aβ-42o and hiPSC-NSC-EVs for 24 hours, we added 300 µl of MTT solution (0.5 mg/ml, Sigma-Aldrich) to each culture well and then incubated them for 4 hours at 37°C. The wells were then treated with 300 µl of DMSO to release the purple formazan into the solution, and we recorded the absorbance at 570 nm. We calculated the percentage of cell viability and compared it across the study groups.

Measurement of cell viability via Live and dead cell assay.

We employed the ReadyProbes™ Cell Viability Imaging Kit (Invitrogen, Waltham, MA, USA) to measure the number of live and dead cells in neuronal cultures. We mixed two drops of NucBlue™ Live

Reagent and NucGreen™ Dead Reagent with 1 ml of neuronal media and added the mixture to neuronal cultures that have been incubated for 24 hours with Aβ-42o and different doses of hiPSC-NSC-EVs. Following incubation of reagents at 37°C for 30 minutes, images were taken in a Nikon inverted fluorescence microscope.

Measurement of the survival of Map-2 positive neurons.

The cultures from all groups (control, Aβ-42o, and Aβ-42o plus hiPSC-NSC-EVs groups) were processed for Map-2 immunofluorescence staining using an antibody against Map2 (ThermoFisher Scientific) and counterstained with DAPI (ThermoFisher Scientific) to assess the number of surviving neurons present in different cultures. Then, neuronal counts per 0.35 mm^2 unit area were taken from randomly chosen 10 images from 3 independent wells.

Quantification of oxidative stress markers.

Three independent neuronal cultures from each group were separately lysed in ice-cold RIPA buffer (Life Technologies, Carlsbad, CA, USA) with protease and phosphatase inhibitor cocktail (Life Technologies) using sonication for 10 seconds. The lysed solution was centrifuged twice, and aliquots of the supernatant solution were stored at -80°C until further use. The protein concentration in different samples was measured using a Pierce BCA reagent kit (ThermoFisher Scientific). We followed the manufacturer's instructions for measuring malondialdehyde (MDA Cayman Chemical; Ann Arbor, MI, USA) and PCs (Cayman Chemical) from neuronal culture lysates.

Measurement of the expression of genes related to oxidative stress and apoptosis in neuronal cultures

We conducted qRT-PCR to measure the expression of genes involved in regulating oxidative stress (iNos and Cox2) and apoptosis (Bad, Bax, and Bcl2) in neuronal cultures from all groups (control, Aβ-42o and Aβ-42o plus hiPSC-NSC-EVs groups, n = 3/group). Total RNA was extracted using the RNeasy kit (Qiagen, Valencia, CA, USA), as outlined in our previous reports [48]. The extracted RNA (500 ng) was then converted to cDNA using the RT2 First Strand Kit (Qiagen) and stored at −20°C until further analysis [48]. The reactions were carried out according to the manufacturer's protocol using a CFX96 Real-Time System (Bio-Rad, Hercules, CA, USA). PCR amplification and melt curve analysis were performed as

detailed in our previous report [48]. Finally, the 2^dd-Ct values for each gene were compared across different groups.

Quantification of proteins levels of BCL-2 and BAD by ELISA.

The selected antiapoptotic and proapoptotic markers BCL2 and BAD levels were measured in neuronal cultures from all groups (control, Aβ-42o, and Aβ-42o plus hiPSC-NSC-EVs groups, n = 3/group). We followed the manufacturer's protocol to measure the protein concentrations of BCL2 (Invitrogen) and BAD (MyBioSource, San Diego, CA, USA) in the cell lysates of neuronal cell cultures.

Measurement of mitochondrial respiration complex genes.

We evaluated the expression of genes linked to different mitochondrial complexes, including complex I (Ndufs6, Ndufs7), complex II (Sdha, Sdhb), complex III (Cyc1, Bcs1l), complex IV (Cox6a1), and complex V (Atp6ap1) in RNA samples extracted from neuronal cultures belonging to different experimental groups (control, Aβ-42o, and Aβ-42o plus hiPSC-NSC-EVs, n = 3/group). We used specific primers (Genecopoeia, Rockville, MD, USA) to amplify the cDNA samples and then normalized the obtained CT values with the housekeeping gene Gapdh. The 2^dd-Ct values for each gene were then compared across the different groups of neuronal cultures.

Measurement of autophagy related protein, beclin1 and MAP1LC3B.

Autophagy is a fundamental process that clears the accumulation and deposition of toxic proteins in the cellular system [49]. We measured autophagy-related markers such as beclin1 (Mybiosource) and MAP1LC3B (Mybiosource) in neuronal cultures belonging to different experimental groups (control, Aβ-42o, and Aβ-42o plus hiPSC-NSC-EVs, n = 3/group).

Quantification of total tau and phospho-tau.

Standard sandwich ELISA protocol was carried out as per the manufacturer's guidelines for the measurement of total tau (Invitrogen) and phospho-tau (Invitrogen) in neuronal cultures belonging to

different experimental groups (control, Aβ-42o, and Aβ-42o + hiPSC-NSC-EVs, n = 3/group). The concentrations of these proteins were normalized to 1 mg of total protein in the cell lysate.

Statistical Analyses.

The experiments utilized 3 independent cultures per condition, and statistical analysis was done using Prism software 10.0. A one-way ANOVA with Newman-Keuls multiple comparison post-hoc tests was employed for datasets containing three or more groups comparison. In all comparisons, $p<0.05$ was considered a statistically significant value.

Results

Establishment of hiPSC-NSCs and primary human neuronal cultures from hiPSC-NSCs.

Incubation of the hiPSC colony (Fig. 1 [A]) with the neurobasal medium containing neural induction supplement for nine days resulted in the generation of cells having small polygonal to spindle-shaped morphology. Subsequent serial passaging of these cells eliminated undifferentiated hiPSCs, and all cells in passage 11 cultures expressed NSC markers Sox-2 and nestin (Fig. 1 [B-D]). Furthermore, hiPSC-NSCs from two different hiPSC lines subjected to neuronal differentiation protocol gave rise to mature neurons expressing markers such as Map-2 and NeuN (Fig. 1 [E-L]). From here onwards, the neurons derived from two distinct hiPSC lines are referred to as iNeurons 1 and iNeurons 2.

[Figure 1 here]

hiPSC-NSC-EVs exhibited a characteristic ultrastructure and expressed CD63, CD81, and Alix.

The SEC fractions 7–13 contained considerably higher numbers of EVs with minimal co-eluting proteins (Fig. 2 [A]); hence, only the fractions 7-13 were pooled and used for further studies. Nanoparticle tracking analysis showed that the size of EVs ranged from 100 to 200 nm with a mean value of 121.6 ± 0.6 nm (Fig. 2 [B]). Imaging with a TEM demonstrated round or oval vesicles with lipid bilayer membranes ranging from 50 to 130 nm in diameter. Examples of individual EVs exhibiting different sizes and shapes found in our hiPSC-NSC-EVs preparations are illustrated in Figure 2 (Fig. 2 [C]).

Additionally, western blot analysis showed that EVs expressed several EV markers, including CD63, CD81, and ALIX (Fig. 2 [D]). The EV preparation lacked the deep cellular protein such as the cytochrome C (Fig. 2 [D]).

***Visualization of the interaction of PKH26-labelled hiPSC-NSC-EVs with mature human neurons exposed to* Aβ-42o**

The experiment involved the addition of PKH26-labeled hiPSC-NSC-EVs to two types of neuronal cultures: one was standard cultures, and the other was exposed to Aβ-42o. The results demonstrated that hiPSC-NSC-EVs could interact with neurons in both cultures. Whether in a standard or adverse environment, the hiPSC-NSC-EVs were observed to either contact the outer membranes of neurons or to be taken up by the neurons themselves, as depicted in Fig. 2 [E-H]. Notably, the presence of Aβ-42o did not disrupt the ability of hiPSC-NSC-EVs to interact with the neurons.

[Figure 2 here]

Aβ-42o induced neurodegeneration in hiPSC-NSC-derived neurons is dose-dependent.

The exposure of mature neurons to different concentrations of Aβ-42o induced significant neurodegeneration (Fig. 3 [A]). Measurement of the percentage neuronal viability using an MTT assay indicated that Aβ-42o induced neurodegeneration is dose-dependent with a lower dose (0.1 µM) causing a moderate decrease in viability ($p<0.05$, Fig. 3 [A]), whereas higher doses (0.5, 1.0, 1.5 or 5 µM) causing much severe, progressive decreases in neuronal viability ($p<0.0001$, Fig. 3 [A]). Exposure to Aβ-42o at 5 µM concentration reduced viability to ~53% of the control group (Fig. 3 [A]). Thus, the subsequent experiments were performed using the sublethal dose of 1 µM Aβ-42o.

hiPSC-NSC-EVs protected human neurons against Aβ-42o induced neurodegeneration.

Increasing doses (1.5, 3, or 6 x 10^9) of hiPSC-NSC-EVs to Aβ-42o exposed human neuronal cultures reduced neurodegeneration. The protective effects were dose-dependent in both iNeuron 1 and iNeuron 2 cultures. In iNeuron 1 cultures, compared to cultures receiving Aβ-42o alone, Aβ-42o exposed neuronal cultures receiving hiPSC-NSC-EVs treatment at 3 or 6 x 10^9 dose displayed better

survival of neurons ($p<0.05$-0.001, Fig. 3 [B]). In iNeuron 2 cultures, hiPSC-NSC-EVs treatment at 1.5, 3, or 6 x 10^9 doses considerably improved the survival of neurons ($p<0.001$-0.0001, Fig. 3 [C]). Furthermore, fluorescence imaging from the live and dead cell assay (Fig. 3 [D-H, J-N]) revealed significantly higher green fluorescence (implying increased cell death) in the Aβ-42o exposure groups compared to control neuronal cultures in both iNeuron 1 and iNeuron 2 cultures (Fig. 3 [D-E, J-K]). AF analysis of green fluorescence using image J from iNeuron 1 and iNeuron 2 cultures demonstrated significantly higher values in Aβ-42o alone group compared to control ($p<0.01$, Fig. 3 [I, O]). Interestingly, in Aβ-42o exposed neuronal cultures receiving 3 or 6 x 10^9 hiPSC-NSC-EVs, AFs of green fluorescence were reduced compared to Aβ-42o alone group ($p<0.01$, Fig. 3 [I, O]). Moreover, these values matched values in the corresponding control neuronal cultures ($p<0.01$, Fig. 3 [I, O]).

[Figure 3 here]

To further confirm the above findings, we quantified the surviving Map2+ neurons (i.e., number of neurons per unit area) in images taken randomly from different neuronal culture groups (Fig. 4 [A-E, G-K]). In both iNeuron 1 and iNeuron 2 cultures, the survival was diminished in all Aβ-42o exposed groups compared to the control group ($p<0.0001$, Fig. 4 [F, L]). However, compared to neuronal cultures exposed to Aβ-42o alone, Aβ-42o exposed neuronal cultures receiving different doses of hiPSC-NSC-EVs displayed increased survival of neurons in a dose-dependent manner (Fig. 4 [F, L]). In iNeuron 1 cultures, compared to neuronal cultures exposed to Aβ-42o alone, cultures receiving hiPSC-NSC-EVs treatment at 3 or 6 x 10^9 doses displayed better survival of neurons ($p<0.05$-0.0001, Fig. 4 [F]). In iNeuron 2 cultures, hiPSC-NSC-EVs treatment at 1.5, 3, or 6 x 10^9 doses considerably improved the survival of neurons ($p<0.05$-0.0001, Fig. 4 [L]). Thus, multiple measures of neuronal survival, such as MTT assay, fractions of live/dead cells, and the extent of surviving MAP2+ neurons, revealed the protective effects of hiPSC-NSC-EVs against Aβ-42o induced neurodegeneration.

[Figure 4 here]

hiPSC-NSC-EVs treatment suppressed oxidative stress in human neurons exposed to Aβ-42o.

Adding Aβ-42o to mature human neuronal cultures increased oxidative stress in neurons. In iNeuron 1 and iNeuron 2 cultures, the concentrations of oxidative stress markers MDA and PCs were

elevated in cultures exposed to Aβ-42o compared to control cultures ($p<0.05$-0.001, Fig. 5 [A-D]). The addition of hiPSC-NSC-EVs to Aβ-42o exposed neuronal cultures dose-dependently decreased the concentrations of MDA and PCs. In iNeuron 1 cultures, compared to cultures exposed to Aβ-42o alone, MDA concentration was reduced with 1.5, 3.0, or 6 x 10^9 doses ($p<0.05$-0.0001, Fig. 5 [A]), and PCs were reduced with the 6 x 10^9 dose ($p<0.05$, Fig. 5 [B]). Moreover, the concentrations of PCs in EVs treated cultures were normalized to control culture levels with all doses of EVs tested ($p>0.05$, Fig. 5 [B]). In iNeuron 2 cultures, compared to cultures exposed to Aβ-42o alone, MDA concentration was reduced with 3.0 or 6 x 10^9 doses ($p<0.05$, Fig. 5 [C]), and PCs were reduced with the 3, or 6 x 10^9 dose ($p<0.05$, Fig. 5 [D]). Furthermore, the concentrations of both MDA and PCs in EVs treated cultures were normalized to control culture levels with all doses of EVs tested ($p>0.05$, Fig. 5 [C-D]).

Next, we measured the expression of genes iNOS and COX-2 in neuronal cultures exposed to Aβ-42o. The genes iNOS and COX-2 encode proteins that are critical enzymes involved in generating ROS. The expression of these genes was increased in neuronal cultures exposed to Aβ-42o alone ($p<0.05$-0.0001, Fig. 5 [E-H]). In both iNeuron 1 and iNeuron 2 cultures, compared to cultures exposed to Aβ-42o alone, the expression of iNOS and COX-2 genes was reduced with all doses of EVs (1.5, 3.0 or 6 x 10^9) tested in the study ($p<0.05$-0.0001, Fig. 5 [E-H]). Furthermore, their expression was normalized to control culture levels with all doses of EVs tested ($p>0.05$, Fig. 5 [E-H]). Thus, measurement of MDA, PCs, and genes iNOS and COX-2 all pointed to reduced oxidative stress in Aβ-42o exposed neuronal cultures treated with hiPSC-NSC-EVs.

hiPSC-NSC-EVs treatment mediated anti-apoptotic effects on human neurons exposed to Aβ-42o.

The expression of pro-apoptotic genes Bad and Bax was increased in human neuronal cultures exposed to Aβ-42o. The increases were significant for both Bad and Bax in iNeuron 1 cultures and for only Bax in iNeuron 2 cultures ($p<0.01$, Fig. 5 [I-J]). In iNeuron 1 cultures, compared to cultures exposed to Aβ-42o alone, the expression of Bad and Bax genes was reduced with all doses of EVs (1.5, 3.0 or 6 x 10^9) tested in the study ($p<0.05$, Fig. 5 [I-J]). In iNeuron 2 cultures, compared to cultures exposed to Aβ-42o alone, the expression of the Bad gene was reduced with 3.0 or 6 x 10^9 EVs, whereas the expression of the Bax gene was reduced with all doses of EVs tested ($p<0.05$-0.01, Fig. 5 [K-L]). Furthermore, the expression of both Bad and Bax genes was normalized to control culture levels with all doses of EVs tested ($p>0.05$, Fig. 5 [K-L]). Consistent with these results, expression of antiapoptotic gene Bcl2 was

reduced in neuronal cultures exposed to Aβ-42o ($p<0.05$) in both iNeuron 1 and iNeuron 2 cultures (Fig. 5 [M, O]). In iNeuron 1 cultures, compared to cultures exposed to Aβ-42o alone, the expression of Bcl-2 gene was increased in cultures treated with hiPSC-NSC-EVs with all doses of EVs (1.5, 3.0, or 6 x 10^9 EVs) tested in the study ($p<0.05$-0.0001, Fig. 5 [M]). In iNeuron 2 cultures, a similar trend was observed, but increases were not significant. However, the expression of Bcl-2 was normalized to control culture levels with all doses of EVs tested in both iNeuron 1 and iNeuron 2 cultures ($p>0.05$, Fig. 5 [M, O]).

We also measured the concentration of BAD and BCL2 proteins to confirm gene expression results, which revealed similar findings. In both iNeuron 1 and iNeuron 2 cultures, compared to controls, the concentration of BAD was increased in cultures exposed to Aβ-42o alone ($p<0.05$) but not in cultures treated with Aβ-42o and different doses of hiPSC-NSC-EVs ($p>0.05$, Fig. 5 [N, P]). Compared to cultures exposed to Aβ-42o alone, the concentration of BAD was decreased with 3.0 or 6 x 10^9 EVs in iNeuron 1 cultures and with all doses of EVs tested in iNeuron 2 cultures ($p<0.05$-0.01, Fig. 5 [N, P]). In both iNeuron 1 and iNeuron 2 cultures, compared to controls, the concentration of BCL2 was decreased in cultures exposed to Aβ-42o alone ($p<0.05$) but not in cultures treated with Aβ-42o and different doses of hiPSC-NSC-EVs ($p>0.05$, Fig. 5 [Q, R]). Compared to cultures exposed to Aβ-42o alone, the concentration of BCL2 was increased with all doses of EVs tested 3.0 or 6 x 10^9 EVs in iNeuron 1 cultures and with 6 x 10^9 EVs in iNeuron 2 cultures ($p<0.05$-0.01, Fig. 5 [Q, R]). Thus, measurement of genes Bad, Bax, and Bcl-2 and proteins BAD and BCL2 supported significant antiapoptotic effects of hiPSC-NSC-EVs on neuronal cultures exposed to Aβ-42o.

[Figure 5 here]

hiPSC-NSC-EVs treatment normalized the expression of genes linked to mitochondrial complex proteins in human neurons exposed to Aβ-42o.

The expression of genes linked to mitochondrial complex such as Ndufs6, Ndufs7 (complex I), Sdha, Sdhb (Complex II), and Atp6ap1 (complex V) were upregulated in neuronal cultures exposed to Aβ-42o ($p<0.05$-0.01, Fig. 6 [A-D, F, H]). However, in Aβ-42o exposed neuronal cultures treated with 6 x 10^9 EVs, their expression levels were normalized to naïve control levels ($p>0.05$, Fig 6 [A-D, F, H]). Furthermore, compared to neuronal cultures exposed to Aβ-42o alone, Aβ-42o exposed neuronal cultures treated with 6 x 10^9 EVs displayed reduced expression of Ndufs6, Ndufs7, Sdha, Sdhb, and

Atp6ap1 ($p<0.05$-0.01, Fig 6 [A-D, F, H]). The expression of genes Cyc1, Bcs1l (Complex III), and Cox6a1 (complex IV) also showed similar trends but were not significant statistically. Thus, genes linked to the mitochondrial electron transport undergo downregulation in human neurons exposed to Aβ-42o, but their expression could be normalized through hiPSC-NSC-EVs treatment.

hiPSC-NSC EVs treatment improved autophagy in human neurons exposed to Aβ-42o.

The concentration of autophagy-related proteins Beclin-1 and MAP1-LC3B were downregulated in human neuronal cultures exposed to Aβ-42o ($p<0.05$-0.01, Fig. 6 [I-J]). However, in Aβ-42o exposed neuronal cultures treated with 6 x 10^9 EVs, their concentrations were normalized to naïve control levels ($p>0.05$, Fig 6 [I-J]). Furthermore, compared to neuronal cultures exposed to Aβ-42o alone, Aβ-42o exposed neuronal cultures treated with 6 x 10^9 EVs displayed increased concentration of Beclin-1 and MAP1-LC3B ($p<0.05$-0.01, Fig 6 [I-J]). Thus, hiPSC-NSC-EVs treatment can normalize autophagy in human neurons exposed to Aβ-42o.

hiPSC-NSC EVs treatment reduced increased tau phosphorylation in human neurons exposed to Aβ-42o.

The concentration of total tau did not change in human neurons exposed to Aβ (Fig. 6 [K]), but the phosphorylation of tau increased with Aβ-42o exposure (Fig. 6 [L]). The concentration of p-tau increased in neuronal cultures exposed to Aβ-42o ($p<0.05$, Fig. 6 [L]). However, in Aβ-42o exposed neuronal cultures treated with 6 x 10^9 EVs, the concentration of p-tau was normalized to the naïve control level ($p>0.05$, Fig 6 [L]). Furthermore, compared to neuronal cultures exposed to Aβ-42o alone, Aβ-42o exposed neuronal cultures treated with 6 x 10^9 EVs displayed reduced concentration of p-tau ($p<0.05$, Fig 6 [L]). Thus, human neurons exposed to Aβ-42o undergo increased tau phosphorylation but hiPSC-NSC-EVs can considerably reduce such adverse change.

[Figure 6 here]

Discussion

The findings of this study underscore the potential of purified and well-characterized hiPSC-NSC-EVs in safeguarding human neurons derived from two distinct hiPSC lines against Aβ-42o induced neurodegeneration. In the context of Aβ-42o induced neurodegeneration, a moderate dose of 1 µM Aβ-42o was selected for neuroprotection experiments, as higher doses were observed to induce more severe neurodegeneration in a dose-dependent manner. The prominent pathological alterations induced by 1 µM Aβ-42o in human neurons encompassed heightened lipid peroxidation and protein oxidation, as indicated by elevated levels of MDA and PCs. Additionally, there was an augmented expression of iNOS and COX-2 genes that encode proteins implicated in ROS generation, increased expression of pro-apoptotic genes and proteins (Bad and Bax), alongside decreased expression of an antiapoptotic gene and protein (Bcl-2). Furthermore, hyperactivation of the mitochondria was evident from the upregulation of genes associated with mitochondrial complexes, including Ndufs6, Ndufs7 (complex I), Sdha, Sdhb (Complex II), and Atp6ap1 (complex V). Moreover, exposure of human neurons to 1 µM Aβ-42o substantially influenced autophagy, leading to reduced concentrations of autophagy-related proteins Beclin-1 and MAP1-LC3B. Additionally, Aβ-42o-exposed human neurons displayed increased tau phosphorylation. Remarkably, introducing hiPSC-NSC-EVs into Aβ-42o-exposed human neuronal cultures provided dose-dependent protection to human neurons through antioxidant and antiapoptotic mechanisms. This protection was evidenced by reduced concentrations of MDA and PCs, reduced expression of iNOS, COX-2, Bad, and Bax, and increased expression of Bcl-2. These effects were also associated with the normalization of gene expression involved in mitochondrial complex proteins and autophagy and the mitigation of tau phosphorylation.

hiPSC-NSC-EVs protected human neurons exposed to Aβ-42o by antioxidant activity and normalizing mitochondrial function

Previous research has reported that Aβ-42o can induce pathological changes and toxicity in rodent neurons. Studies have indicated that Aβ42o can negatively impact Ca^{2+} homeostasis in neurons by promoting increased Ca^{2+} entry [50]. Depending on the dosage, this effect may result in a significant Ca^{2+} influx and excitotoxicity [51,52]. Aβ-42o is also able to integrate into the lipid bilayer, acting as a source of ROS and initiating lipid peroxidation [23–25]. This membrane lipid peroxidation can disrupt neuronal Ca^{2+} homeostasis, leading to Ca^{2+} overload and neurodegeneration [53]. Studies have also

shown that Aβ-42o can form pore-like structures (also referred to as amyloid channels) in neuronal membranes causing increased Ca^{2+} permeability, disruption of Ca^{2+} homeostasis, and eventually neurodegeneration [50,54]. Furthermore, Aβ-42o could accumulate in mitochondrial membranes, leading to a reduction in mitochondrial membrane potential. This accumulation also disrupts the transportation of nuclear-encoded mitochondrial proteins to mitochondria, interferes with the electron transport chain, increases the production of ROS, and results in damage to the mitochondria [26]. Moreover, exposure of neurons to Aβ-42o can lead to a decrease in mitochondrial superoxide dismutase 2 and mitochondrial cytochrome C protein levels [27]. While the current study did not explore altered Ca^{2+} homeostasis, it did observe increased lipid peroxidation in human neurons exposed to Aβ-42o, as evidenced by elevated MDA concentration. An overall increase in oxidative stress was also apparent from enhanced levels of PCs and iNOS. iNOS is expressed only during pathophysiological states, and the nitric oxide produced by iNOS enhances the production of ROS [55]. The elevated expression of Cox-2 also indicated increased oxidative stress in human neurons exposed to Aβ-42o. Neurons are particularly susceptible to damage caused by free radicals generated through COX-2 peroxidase activity [56].

Notably, the addition of hiPSC-NSC-EVs into Aβ-42o-exposed human neuronal cultures protected them by significantly reducing lipid peroxidation, as evidenced by decreased MDA levels, and overall oxidative stress, as observed from the reduced expression of PCs, iNOS, and COX-2. These antioxidant effects of hiPSC-NSC-EVs may be attributed to specific miRNAs and protein cargo they carry. For example, hiPSC-NSC-EVs are enriched with miRNA-181 and hemopexin, which can maintain mitochondrial function and homeostasis [43], as well as reducing ROS toxicity [36,44]. Indeed, increased mitochondrial activity in human neurons exposed to Aβ-42o was normalized by hiPSC-NSC-EVs treatment in this study. Such modulation could be gleaned from the expression of genes linked to mitochondrial complexes I (Ndufs6, Ndufs7), II (Sdha, Sdhb), and IV (Atp6ap1) in human neurons exposed to Aβ-42o and hiPSC-NSC-EVs to levels seen in naive human neurons. Thus, antioxidant and mitochondria protecting effects are among the mechanisms by which hiPSC-NSC-EVs protected human neurons exposed to Aβ-42o.

hiPSC-NSC-EVs protected human neurons exposed to Aβ-42o by antiapoptotic effects

Exposure of neurons to Aβ-42o results in apoptosis, which involves altered expression of pro- and anti-apoptotic proteins [29]. Particularly, mitochondrial-specific accumulation of Aβ-42o induces

mitochondrial dysfunction causing apoptotic cell death [28]. Indeed, in this study, the neurodegeneration occurring through apoptosis was evident from increased expression of pro-apoptotic genes and proteins Bad and Bax, alongside decreased expression of an antiapoptotic gene and protein (Bcl-2). This is consistent with the Bax and Bad upregulation and Bcl-2 downregulation found in hippocampal slice cultures exposed to Aβ-42o [57] and altered expression of these proteins within neurons in AD [58]. Bax promotes apoptosis by translocating into the mitochondrial membrane and facilitating cytochrome c release whereas Bad induces the activation of Bax, by inactivating the pro-survival Bcl-2 protein. Bcl-2 prevents apoptotic death in multiple cell types including neurons [59]. Bcl-2 prevents the permeabilization of mitochondria to inhibit Ca^{2+} overload and consequently the activity of cleaved caspases, whereas Bax exerts the opposite effects [60].

However, the extent of apoptosis was reduced after introducing hiPSC-NSC-EVs into Aβ-42o-exposed human neuronal cultures. Such a reduction could be ascertained from the decreased expression of Bad and Bax and increased expression of Bcl-2. In this study, the downregulation of Bax by hiPSC-NSC-EVs is likely the most crucial antiapoptotic mechanism, as previous study has shown that the suppression of Aβ-42o-mediated neurotoxicity can be significantly achieved through the inhibition of Bax activity, either genetically or pharmacologically [57]. Additionally, the antiapoptotic effects of hiPSC-NSC-EVs are likely due to miRNA-103a and miRNA-21-5p, as well as a protein called pentraxin-3 carried by them, as they can promote neuroprotection through antiapoptotic mechanisms. [39–42]. The role of miRNA-103a in inhibiting apoptosis has been observed in several studies. One study demonstrated that during hypoxia/reoxygenation conditions, overexpression of miRNA-103a in cardiomyocytes significantly reduced apoptosis by inhibiting Bax, cleaved caspase-3, and cleaved caspase-9 [61]. Another study showed that in nerve growth factor-stimulated PC12 cells and primary cerebral cortical neurons exposed to Aβ-42o, overexpression of miRNA-103 resulted in decreased apoptosis associated with reduced expression of cleaved caspase-3, while inhibition of miRNA-103 led to increased apoptosis [42]. Further analysis indicated that miRNA-103 exerts antiapoptotic effects by targeting prostaglandin-endoperoxide synthase 2, a protein that plays a significant role in AD development and progression [42]. Thus, hiPSC-NSC EVs enriched with miRNA-103a have the potential for mitigating neurodegeneration in AD. This is particularly important given that miRNA-103 is downregulated in AD patients and models [62,63], indicating its involvement in the pathogenesis of AD.

Additionally, miRNA-21-5p, found in abundance in hiPSC-NSC-EVs, likely also played a role in mitigating apoptosis because an earlier investigation using SH-SY5Y cells showed that miRNA-21 can

significantly diminish apoptosis induced by Aβ-42o. Such effect was associated with the inhibition of Bax and programmed cell death protein 4, alongside an elevation in Bcl-2 [64]. Furthermore, the contribution of pentraxin-3 protein within hiPSC-NSC-EVs to antiapoptotic properties cannot be ruled out since a previous study utilizing a mouse model of Parkinson's disease revealed that treatment with human recombinant pentraxin-3 can prevent apoptosis and degeneration of dopaminergic neurons [65]. Considering these findings, it is conceivable that the enrichment of miRNA-103a, miRNA-21-5p, and pentraxin-3 in hiPSC-NSC-EVs has significantly attenuated apoptosis in human neurons exposed to Aβ-42o in this study. However, establishing a definitive cause-and-effect relationship would necessitate further investigations utilizing naïve EVs loaded with these miRNAs or pentraxin-3.

hiPSC-NSC-EVs reduced tau phosphorylation and improved autophagy in Aβ-42o exposed human neurons

Aβ-42o exposures to neurons elicit a substantial increase in tau protein phosphorylation. For instance, the administration of Aβ-42o into the brains of mice induces a marked rise in the number of NFTs proximal to the injection sites [66]. Therefore, it is likely that Aβ-42o operates upstream of tau, instigating a cascade that culminates in tau-dependent synaptic dysfunction [67,68]. Aβ-42o exposure augments tau phosphorylation through the activation of tau kinases mitogen-activated protein kinase and glycogen synthase kinase-3 beta [30,31]. Furthermore, a study suggested that heightened ROS production after Aβ-42o exposure initiates mechanistic target of rapamycin C1 (mTORC1) activation [69]. Subsequent mTORC1 elevation inhibits autophagy and stimulates the expression of cell cycle regulatory proteins such as cyclin-dependent kinase 2 (CDK2), which interacts with tau, inducing tau phosphorylation and microtubule destabilization during neurodegeneration [69]. These findings align with the decreased concentration of autophagy-related proteins Beclin 1 and MAP1LC3B and increased tau phosphorylation observed in the present study.

Introducing hiPSC-NSC-EVs into Aβ-42o-exposed human neuronal cultures improved autophagy and reduced tau phosphorylation. It remains to be investigated how hiPSC-NSC-EVs improve autophagy and decrease tau phosphorylation in human neurons exposed to Aβ-42o. However, it is worth noting that hiPSC-NSC-EVs carry miRNA-122, which can improve autophagy [36]. A study has shown that overexpression of miRNA-122 leads to increased cell-protective autophagy characterized by the lipidation of LC3B and corresponding consumption of p62, and miRNA-122 knockdown inhibited

autophagy [70]. Moreover, miRNA-148a-3p may be involved in tau phosphorylation, as this miRNA is enriched in hiPSC-NSC-EVs [36]. The potential role of miRNA-148-3a in inhibiting tau phosphorylation is evident from a study demonstrating that the downregulation of miRNA-148a-3p leads to tau hyperphosphorylation and the progression of AD [71]. Additional analysis revealed that miRNA-148a-3p targets CDK-5 regulatory subunit 1 and phosphatase and tensin homolog deleted on chromosome 10 (PTEN) involved in tau hyperphosphorylation. Moreover, a strategy enhancing miRNA-148a-3p signaling reduced tau hyperphosphorylation in AD mice [71].

Conclusions

The results of this study emphasize the potential of hiPSC-NSC-EVs in protecting human neurons derived from two distinct hiPSC lines against neurodegeneration induced by Aβ-42o. Importantly, when hiPSC-NSC-EVs were introduced into Aβ-42o-exposed human neuronal cultures, they provided protection to human neurons in a manner that depended on the dosage. This protection was observed to be mediated mainly through antioxidant and antiapoptotic mechanisms. The evidence for such a mechanism included reduced levels of multiple oxidative stress, proapoptotic and mitochondrial hyperactivation markers, and increased expression of genes and/or proteins that inhibit apoptosis. Furthermore, these beneficial effects were also associated with normalized autophagy and decreased tau phosphorylation. These findings encourage investigating whether administering hiPSC-NSC-EVs in AD models would provide significant neuroprotection and slow AD pathogenesis in future studies.

Acknowledgments

The TEM images of hiPSC-NSC-EVs were taken at the Image Analysis Laboratory, Texas A&M Veterinary Medicine & Biomedical Sciences (RRIS: SCR_0222479).

Availability of data and materials

Data supporting this study are included within the article.

Funding

Supported by grants from the National Institutes for Aging (1RF1AG074256-01 and R01AG075440-01 to A.K.S.) and National Institute for Neurological Disorders and Stroke (1R01NS106907-05 to A.K.S.).

Authors' contributions

Concept: AKS. Research design: AKS, SR, and LNM. Data collection, analysis, and interpretation: SR, LNM, RSB, AN, RU, EN and AKS. Preparation of figure composites: SR and LNM. Manuscript writing: SR, LNM, and AKS. All authors provided feedback, edits, and additions to the manuscript text and approved the final version of the manuscript.

Declarations:

Ethics declarations: Not applicable as this study did not involve human or animal subjects.
Other declarations: The authors declare that they have not used Artificial Intelligence in this study.

Conflicts of interest

The authors confirm that they have no conflicts of interest.

Consent for publication

All necessary consent and approvals were obtained from all authors and co-authors.

References

1. 2024 Alzheimer's disease facts and figures. Alzheimers Dement J Alzheimers Assoc. 2024; 20:3708–821.
2. Hebert LE, Weuve J, Scherr PA, Evans DA. Alzheimer disease in the United States (2010-2050) estimated using the 2010 census. Neurology. 2013; 80:1778–83.
3. Hampel H, Hardy J, Blennow K, Chen C, Perry G, Kim SH, et al. The Amyloid-β Pathway in Alzheimer's Disease. Mol Psychiatry. 2021; 26:5481–503.
4. Yarns BC, Holiday KA, Carlson DM, Cosgrove CK, Melrose RJ. Pathophysiology of Alzheimer's Disease. Psychiatr Clin North Am. 2022; 45:663–76.
5. Moore KBE, Hung T-J, Fortin JS. Hyperphosphorylated tau (p-tau) and drug discovery in the context of Alzheimer's disease and related tauopathies. Drug Discov Today. 2023; 28:103487.
6. Guarnieri L, Bosco F, Leo A, Citraro R, Palma E, De Sarro G, et al. Impact of micronutrients and nutraceuticals on cognitive function and performance in Alzheimer's disease. Ageing Res Rev. 2024; 95:102210.
7. Sun H-L, Chen S-H, Yu Z-Y, Cheng Y, Tian D-Y, Fan D-Y, et al. Blood cell-produced amyloid-β induces cerebral Alzheimer-type pathologies and behavioral deficits. Mol Psychiatry. 2021; 26:5568–77.
8. Blennow K, de Leon MJ, Zetterberg H. Alzheimer's disease. Lancet Lond Engl. 2006; 368:387–403.
9. Kulenkampff K, Wolf Perez A-M, Sormanni P, Habchi J, Vendruscolo M. Quantifying misfolded protein oligomers as drug targets and biomarkers in Alzheimer and Parkinson diseases. Nat Rev Chem. 2021; 5:277–94.
10. Brody DL, Jiang H, Wildburger N, Esparza TJ. Non-canonical soluble amyloid-beta aggregates and plaque buffering: controversies and future directions for target discovery in Alzheimer's disease. Alzheimers Res Ther. 2017; 9:62.
11. Hampel H, Hu Y, Hardy J, Blennow K, Chen C, Perry G, et al. The amyloid-β pathway in Alzheimer's disease: a plain language summary. Neurodegener Dis Manag. 2023; 13:141–9.
12. Wilhelm BG, Mandad S, Truckenbrodt S, Kröhnert K, Schäfer C, Rammner B, et al. Composition of isolated synaptic boutons reveals the amounts of vesicle trafficking proteins. Science. 2014; 344:1023–8.

13. Rice HC, de Malmazet D, Schreurs A, Frere S, Van Molle I, Volkov AN, et al. Secreted amyloid-β precursor protein functions as a GABABR1a ligand to modulate synaptic transmission. Science. 2019;363: eaao4827.
14. Shankar GM, Li S, Mehta TH, Garcia-Munoz A, Shepardson NE, Smith I, et al. Amyloid-beta protein dimers isolated directly from Alzheimer's brains impair synaptic plasticity and memory. Nat Med. 2008; 14:837–42.
15. Brinkmalm G, Hong W, Wang Z, Liu W, O'Malley TT, Sun X, et al. Identification of neurotoxic cross-linked amyloid-β dimers in the Alzheimer's brain. Brain J Neurol. 2019; 142:1441–57.
16. Li S, Selkoe DJ. A mechanistic hypothesis for the impairment of synaptic plasticity by soluble Aβ oligomers from Alzheimer's brain. J Neurochem. 2020; 154:583–97.
17. Selkoe DJ. Soluble oligomers of the amyloid beta-protein impair synaptic plasticity and behavior. Behav Brain Res. 2008; 192:106–13.
18. Hartley DM, Walsh DM, Ye CP, Diehl T, Vasquez S, Vassilev PM, et al. Protofibrillar intermediates of amyloid beta-protein induce acute electrophysiological changes and progressive neurotoxicity in cortical neurons. J Neurosci Off J Soc Neurosci. 1999; 19:8876–84.
19. Lewis J, Dickson DW, Lin WL, Chisholm L, Corral A, Jones G, et al. Enhanced neurofibrillary degeneration in transgenic mice expressing mutant tau and APP. Science. 2001; 293:1487–91.
20. Wang L, Benzinger TL, Su Y, Christensen J, Friedrichsen K, Aldea P, et al. Evaluation of Tau Imaging in Staging Alzheimer Disease and Revealing Interactions Between β-Amyloid and Tauopathy. JAMA Neurol. 2016; 73:1070–7.
21. He Z, Guo JL, McBride JD, Narasimhan S, Kim H, Changolkar L, et al. Amyloid-β plaques enhance Alzheimer's brain tau-seeded pathologies by facilitating neuritic plaque tau aggregation. Nat Med. 2018; 24:29–38.
22. Busche MA, Hyman BT. Synergy between amyloid-β and tau in Alzheimer's disease. Nat Neurosci. 2020; 23:1183–93.
23. Butterfield DA, Drake J, Pocernich C, Castegna A. Evidence of oxidative damage in Alzheimer's disease brain: central role for amyloid beta-peptide. Trends Mol Med. 2001; 7:548–54.
24. Butterfield DA, Castegna A, Lauderback CM, Drake J. Evidence that amyloid beta-peptide-induced lipid peroxidation and its sequelae in Alzheimer's disease brain contribute to neuronal death. Neurobiol Aging. 2002; 23:655–64.

25. Butterfield DA, Swomley AM, Sultana R. Amyloid β-peptide (1-42)-induced oxidative stress in Alzheimer disease: importance in disease pathogenesis and progression. Antioxid Redox Signal. 2013; 19:823–35.
26. Reddy PH, Beal MF. Amyloid beta, mitochondrial dysfunction and synaptic damage: implications for cognitive decline in aging and Alzheimer's disease. Trends Mol Med. 2008; 14:45–53.
27. Olajide OJ, La Rue C, Bergdahl A, Chapman CA. Inhibiting amyloid beta (1-42) peptide-induced mitochondrial dysfunction prevents the degradation of synaptic proteins in the entorhinal cortex. Front Aging Neurosci. 2022; 14:960314.
28. Cha M-Y, Han S-H, Son SM, Hong H-S, Choi Y-J, Byun J, et al. Mitochondria-specific accumulation of amyloid β induces mitochondrial dysfunction leading to apoptotic cell death. PloS One. 2012;7: e34929.
29. Yao M, Nguyen T-VV, Pike CJ. Beta-amyloid-induced neuronal apoptosis involves c-Jun N-terminal kinase-dependent downregulation of Bcl-w. J Neurosci Off J Soc Neurosci. 2005; 25:1149–58.
30. Busciglio J, Lorenzo A, Yeh J, Yankner BA. beta-amyloid fibrils induce tau phosphorylation and loss of microtubule binding. Neuron. 1995; 14:879–88.
31. Zheng W-H, Bastianetto S, Mennicken F, Ma W, Kar S. Amyloid beta peptide induces tau phosphorylation and loss of cholinergic neurons in rat primary septal cultures. Neuroscience. 2002; 115:201–11.
32. Bonetto V, Grilli M. Neural stem cell-derived extracellular vesicles: mini players with key roles in neurogenesis, immunomodulation, neuroprotection and aging. Front Mol Biosci. 2023; 10:1187263.
33. Hering C, Shetty AK. Extracellular vesicles derived from neural stem cells, astrocytes, and microglia as therapeutics for easing TBI-induced brain dysfunction. Stem Cells Transl Med. 2023; 12:140–53.
34. Chang J, Feng Z, Li Y, Lv H, Liu S, Luo Y, et al. Mesenchymal stem cell-derived extracellular vesicles: A novel promising neuroprotective agent for Alzheimer's disease. Biochem Pharmacol. 2024; 222:116064.
35. Xiong Y, Lou P, Xu C, Han B, Liu J, Gao J. Emerging role of ex vesicles in veterinary practice: novel opportunities and potential challenges. Front Vet Sci. 2024; 11:1335107.

36. Upadhya R, Madhu LN, Attaluri S, Gitaí DLG, Pinson MR, Kodali M, et al. Extracellular vesicles from human iPSC-derived neural stem cells: miRNA and protein signatures, and anti-inflammatory and neurogenic properties. J Extracell Vesicles. 2020; 9:1809064.
37. Upadhya R, Madhu LN, Rao S, Shetty AK. Proficiency of Extracellular Vesicles From hiPSC-Derived Neural Stem Cells in Modulating Proinflammatory Human Microglia: Role of Pentraxin-3 and miRNA-21-5p. Front Mol Neurosci. 2022; 15:845542.
38. Ayyubova G, Kodali M, Upadhya R, Madhu LN, Attaluri S, Somayaji Y, et al. Extracellular vesicles from hiPSC-NSCs can prevent peripheral inflammation-induced cognitive dysfunction with inflammasome inhibition and improved neurogenesis in the hippocampus. J Neuroinflammation. 2023; 20:297.
39. Buller B, Liu X, Wang X, Zhang RL, Zhang L, Hozeska-Solgot A, et al. MicroRNA-21 protects neurons from ischemic death. FEBS J. 2010; 277:4299–307.
40. Han Z, Chen F, Ge X, Tan J, Lei P, Zhang J. miR-21 alleviated apoptosis of cortical neurons through promoting PTEN-Akt signaling pathway in vitro after experimental traumatic brain injury. Brain Res. 2014; 1582:12–20.
41. Rodriguez-Grande B, Varghese L, Molina-Holgado F, Rajkovic O, Garlanda C, Denes A, et al. Pentraxin 3 mediates neurogenesis and angiogenesis after cerebral ischaemia. J Neuroinflammation. 2015;24; 12:15.
42. Yang H, Wang H, Shu Y, Li X. miR-103 Promotes Neurite Outgrowth and Suppresses Cells Apoptosis by Targeting Prostaglandin-Endoperoxide Synthase 2 in Cellular Models of Alzheimer's Disease. Front Cell Neurosci. 2018; 12:91.
43. Indrieri A, Carrella S, Romano A, Spaziano A, Marrocco E, Fernandez-Vizarra E, et al. miR-181a/b downregulation exerts a protective action on mitochondrial disease models. EMBO Mol Med. 2019;11: e8734.
44. Hahl P, Davis T, Washburn C, Rogers JT, Smith A. Mechanisms of neuroprotection by hemopexin: modeling the control of heme and iron homeostasis in brain neurons in inflammatory states. J Neurochem. 2013; 125:89–101.
45. Attaluri S, Jaimes Gonzalez J, Kirmani M, Vogel AD, Upadhya R, Kodali M, et al. Intranasally administered extracellular vesicles from human induced pluripotent stem cell-derived neural stem cells quickly incorporate into neurons and microglia in 5xFAD mice. Front Aging Neurosci. 2023; 15:1200445.

46. Madhu LN, Attaluri S, Kodali M, Shuai B, Upadhya R, Gitai D, et al. Neuroinflammation in Gulf War Illness is linked with HMGB1 and complement activation, which can be discerned from brain-derived extracellular vesicles in the blood. Brain Behav Immun. 2019; 81:430–43.
47. Kodali M, Madhu LN, Reger RL, Milutinovic B, Upadhya R, Gonzalez JJ, et al. Intranasally administered human MSC-derived extracellular vesicles inhibit NLRP3-p38/MAPK signaling after TBI and prevent chronic brain dysfunction. Brain Behav Immun. 2023; 108:118–34.
48. Shetty AK, Attaluri S, Kodali M, Shuai B, Shetty GA, Upadhya D, et al. Monosodium luminol reinstates redox homeostasis, improves cognition, mood and neurogenesis, and alleviates neuro- and systemic inflammation in a model of Gulf War Illness. Redox Biol. 2020; 28:101389.
49. Boland B, Kumar A, Lee S, Platt FM, Wegiel J, Yu WH, et al. Autophagy induction and autophagosome clearance in neurons: relationship to autophagic pathology in Alzheimer's disease. J Neurosci Off J Soc Neurosci. 2008; 28:6926–37.
50. Demuro A, Parker I, Stutzmann GE. Calcium signaling and amyloid toxicity in Alzheimer disease. J Biol Chem. 2010; 285:12463–8.
51. Alberdi E, Sánchez-Gómez MV, Cavaliere F, Pérez-Samartín A, Zugaza JL, Trullas R, et al. Amyloid beta oligomers induce Ca2+ dysregulation and neuronal death through activation of ionotropic glutamate receptors. Cell Calcium. 2010; 47:264–72.
52. De Felice FG, Velasco PT, Lambert MP, Viola K, Fernandez SJ, Ferreira ST, et al. Abeta oligomers induce neuronal oxidative stress through an N-methyl-D-aspartate receptor-dependent mechanism that is blocked by the Alzheimer drug memantine. J Biol Chem. 2007; 282:11590–601.
53. Camandola S, Mattson MP. Aberrant subcellular neuronal calcium regulation in aging and Alzheimer's disease. Biochim Biophys Acta. 2011; 1813:965–73.
54. Kawahara M, Ohtsuka I, Yokoyama S, Kato-Negishi M, Sadakane Y. Membrane Incorporation, Channel Formation, and Disruption of Calcium Homeostasis by Alzheimer's β-Amyloid Protein. Int J Alzheimers Dis. 2011; 2011:304583.
55. Zanzinger J. Mechanisms of action of nitric oxide in the brain stem: role of oxidative stress. Auton Neurosci Basic Clin. 2002; 98:24–7.
56. Minghetti L. Cyclooxygenase-2 (COX-2) in inflammatory and degenerative brain diseases. J Neuropathol Exp Neurol. 2004; 63:901–10.
57. Kudo W, Lee H-P, Smith MA, Zhu X, Matsuyama S, Lee H-G. Inhibition of Bax protects neuronal cells from oligomeric Aβ neurotoxicity. Cell Death Dis. 2012 17;3(5): e309

58. Kitamura Y, Shimohama S, Kamoshima W, Ota T, Matsuoka Y, Nomura Y, et al. Alteration of proteins regulating apoptosis, Bcl-2, Bcl-x, Bax, Bak, Bad, ICH-1 and CPP32, in Alzheimer's disease. Brain Res. 1998; 780:260–9.
59. Zörnig M, Hueber A, Baum W, Evan G. Apoptosis regulators and their role in tumorigenesis. Biochim Biophys Acta. 2001;1551: F1-37.
60. Nishihara M, Miura T, Miki T, Tanno M, Yano T, Naitoh K, et al. Modulation of the mitochondrial permeability transition pore complex in GSK-3beta-mediated myocardial protection. J Mol Cell Cardiol. 2007; 43:564–70.
61. Zhang C, Zhang C, Wang H, Qi Y, Kan Y, Ge Z. Effects of miR-103a-3p on the autophagy and apoptosis of cardiomyocytes by regulating Atg5. Int J Mol Med. 2019; 43:1951–60.
62. Chang W-S, Wang Y-H, Zhu X-T, Wu C-J. Genome-Wide Profiling of miRNA and mRNA Expression in Alzheimer's Disease. Med Sci Monit Int Med J Exp Clin Res. 2017; 23:2721–31.
63. Huynh RA, Mohan C. Alzheimer's Disease: Biomarkers in the Genome, Blood, and Cerebrospinal Fluid. Front Neurol. 2017; 8:102.
64. Feng M-G, Liu C-F, Chen L, Feng W-B, Liu M, Hai H, et al. MiR-21 attenuates apoptosis-triggered by amyloid-β via modulating PDCD4/ PI3K/AKT/GSK-3β pathway in SH-SY5Y cells. Biomed Pharmacother Biomedecine Pharmacother. 2018; 101:1003–7.
65. Lian C, Huang Q, Zhong X, He Z, Liu B, Zeng H, et al. Pentraxin 3 secreted by human adipose-derived stem cells promotes dopaminergic neuron repair in Parkinson's disease via the inhibition of apoptosis. FASEB J Off Publ Fed Am Soc Exp Biol. 2021;35: e21748.
66. Götz J, Chen F, van Dorpe J, Nitsch RM. Formation of neurofibrillary tangles in P301l tau transgenic mice induced by Abeta 42 fibrils. Science. 2001; 293:1491–5.
67. Roberson ED, Scearce-Levie K, Palop JJ, Yan F, Cheng IH, Wu T, et al. Reducing endogenous tau ameliorates amyloid beta-induced deficits in an Alzheimer's disease mouse model. Science. 2007; 316:750–4.
68. Bloom GS. Amyloid-β and tau: the trigger and bullet in Alzheimer disease pathogenesis. JAMA Neurol. 2014; 71:505–8.
69. Lee KH, Lee S-J, Lee HJ, Choi GE, Jung YH, Kim DI, et al. Amyloid β1-42 (Aβ1-42) Induces the CDK2-Mediated Phosphorylation of Tau through the Activation of the mTORC1 Signaling Pathway While Promoting Neuronal Cell Death. Front Mol Neurosci. 2017; 10:229.
70. Wang Y, Zhao H, Guo M, Fei D, Zhang L, Xing M. Targeting the miR-122/PKM2 autophagy axis relieves arsenic stress. J Hazard Mater. 2020; 383:121217.

71. Zeng L, Jiang H, Ashraf GM, Liu J, Wang L, Zhao K, et al. Implications of miR-148a-3p/p35/PTEN signaling in tau hyperphosphorylation and autoregulatory feedforward of Akt/CREB in Alzheimer's disease. Mol Ther Nucleic Acids. 2022; 27:256–75.

Figure Legends

Figure 1: Generation and characterization of human neural stem cells (NSCs) and human neurons from human induced pluripotent stem cells (hiPSCs). Figure A shows a hiPSC colony. Images B-D show the expression of nestin (B), Sox-2 (C), and both nestin and Sox-2 counterstained with DAPI (D) in NSCs derived from hiPSCs. Figures E-H and I-J respectively illustrate mature neurons derived hiPSC lines 1 and 2 (iNeurons 1 and 2) immunostained with microtubule-associated protein-2 (MAP-2; E-F, I-J) and neuron-specific nuclear antigen (NeuN; G-H, K-L). Scale bars: 100 µm.

Figure 2: Characterization of extracellular vesicles from human induced pluripotent stem cell-derived neural stem cells (hiPSC-NSC-EVs). Graph A illustrates the number of EVs vis-a-vis protein content in various fractions collected from size-exclusion chromatography. Graph B shows that the average size of EVs varied between 100-200 nm, with a mean size of 121.6 nm. Figure C illustrates the morphology of EVs examined through transmission electron microscopy. Scale bar, 100 nm. Figure D shows the expression of CD63, CD81, and ALIX but not cytochrome C in hiPSC-NSC-EVs visualized through Western blotting. Full-length blots of CD63, CD81, ALIX and cytochrome C are presented in Supplementary figures 1-4. Figures E-H demonstrate the incorporation of PKH26-labeled EVs (red particles) into microtubule-associated protein-2 (MAP-2)-positive human neurons (green) in standard cultures (E-F) and Aβ-42 oligomers exposed cultures (G-H). Scale bar, 100 µm.

Figure 3: Assessment of cell viability in iNeurons cultures exposed to Aβ-42 oligomers (Aβ-42o), or Aβ-42o and extracellular vesicles from human induced pluripotent stem cell-derived neural stem cells (hiPSC-NSC-EVs). The bar chart in A shows the results of an MTT assay comparing the percentages of viable neurons in iNeurons cultures exposed to different concentrations of Aβ-42o. The bar charts B-C show the results of MTT assays comparing the percentages of viable neurons in iNeurons 1 and 2 cultures exposed to Aβ-42o or Aβ-42o and different concentrations of hiPSC-NSC-EVs. Figures D-H and J-N are representative images from cultures of iNeurons 1 (D-H) and iNeurons 2 (J-N), processed for live and dead cell assay. D and J, control iNeurons 1 and 2 cultures. E and K, iNeurons 1 and 2 cultures exposed to Aβ-42o. F and L, iNeurons 1 and 2 cultures exposed to Aβ-42o and treated with 1.5 x 10^9 billion EVs. G and M, iNeurons 1 and 2 cultures exposed to Aβ-42o and treated with 3.0 x 10^9 billion EVs. H and N, iNeurons 1 and 2 cultures exposed to Aβ-42o and treated with 6.0 x 10^9 billion EVs. The bar

charts I and O compare the area fractions of green fluorescence (implying dead cells) across different groups for iNeurons 1 (I) and iNeurons 2 (O) cultures; Scale bar, 100 µm.

Figure 4: The effects of adding extracellular vesicles from human induced pluripotent stem cell-derived neural stem cells (hiPSC-NSC-EVs) into iNeurons cultures on Aβ-42 oligomers (Aβ-42o)-induced neurodegeneration. Figures A-E and H-L show representative images of surviving microtubule-associated protein-2 (MAP-2) positive neurons from control cultures of iNeurons 1 and 2 (A, G), and iNeurons 1 and 2 cultures exposed to Aβ-42o alone (B, H), Aβ-42o and treated with 1.5 x 10^9 billion EVs (C, I), Aβ-42o and treated with 3.0 x 10^9 billion EVs (D, J), or Aβ-42o and treated with 6.0 x 10^9 billion EVs (E, K). Scale bar, 100 µm. The bar charts in F and L compare the numbers of surviving MAP-2+ neurons per unit area (0.35mm^2) of iNeurons 1 and iNeurons 2 cultures across various groups.

Figure 5: The effects of adding extracellular vesicles from human induced pluripotent stem cell-derived neural stem cells (hiPSC-NSC-EVs) into iNeurons cultures on Aβ-42 oligomers (Aβ-42o)-induced oxidative stress and pro-apoptotic gene and protein expression. The bar charts A-D compare the concentrations of malondialdehyde (MDA, A, C) and protein carbonyls (B, D) in Aβ-42o exposed cultures of iNeuron 1 (A-B) and iNeuron 2 (C-D) treated with different concentrations of hiPSC-NSC-EVs. The bar charts E-H compare the relative gene expression of iNos (E, G) and Cox2 (F, H) in Aβ-42o exposed cultures of iNeurons 1 (E-F) and iNeurons 2 (G-H) treated with different concentrations of hiPSC-NSC-EVs. The bar charts I-M and O compare the relative gene expression of Bad (I, K), Bax (J, L), and Bcl2 (M, O) in Aβ-42o exposed cultures of iNeurons 1 (I-J and M) and iNeurons 2 (K-L and O) treated with different concentrations of hiPSC-NSC-EVs. The bar charts N, Q, P, and R compare the protein concentrations of BAD (N, P) and BCL2 (Q, R) in Aβ-42o exposed cultures of iNeurons 1 (N, Q) and iNeurons 2 (P, R) treated with different concentrations of hiPSC-NSC-EVs.

Figure 6: The effects of adding extracellular vesicles from human induced pluripotent stem cell-derived neural stem cells (hiPSC-NSC-EVs) into iNeurons cultures on Aβ-42 oligomers (Aβ-42o)-induced increase in the expression of genes encoding mitochondrial complex proteins, decrease in autophagy-related proteins and tau phosphorylation. The bar charts A-H compare the relative expression of genes Ndufs6 (A), Ndufs7 (B), Sdha (C), Sdhb (D), Cyc1 (E), Bcs1l (F), Cox6a1 (G) and Atp6ap1 (H) in Aβ-42o exposed cultures of iNeurons 1 treated with 6 x 10^9 hiPSC-NSC-EVs. The bar charts I and J compare the concentrations autophagy-related proteins Beclin 1 (I) and MAP1LC3B (J) in Aβ-42o exposed cultures of iNeurons 1 treated with 6 x 10^9 hiPSC-NSC-EVs. The bar charts K and L

compare the concentrations of total tau (K) and phosphorylated-tau (p-tau, L) in Aβ-42o exposed cultures of iNeurons 1 treated with 6 x 10^9 hiPSC-NSC-EVs.

Figure 1

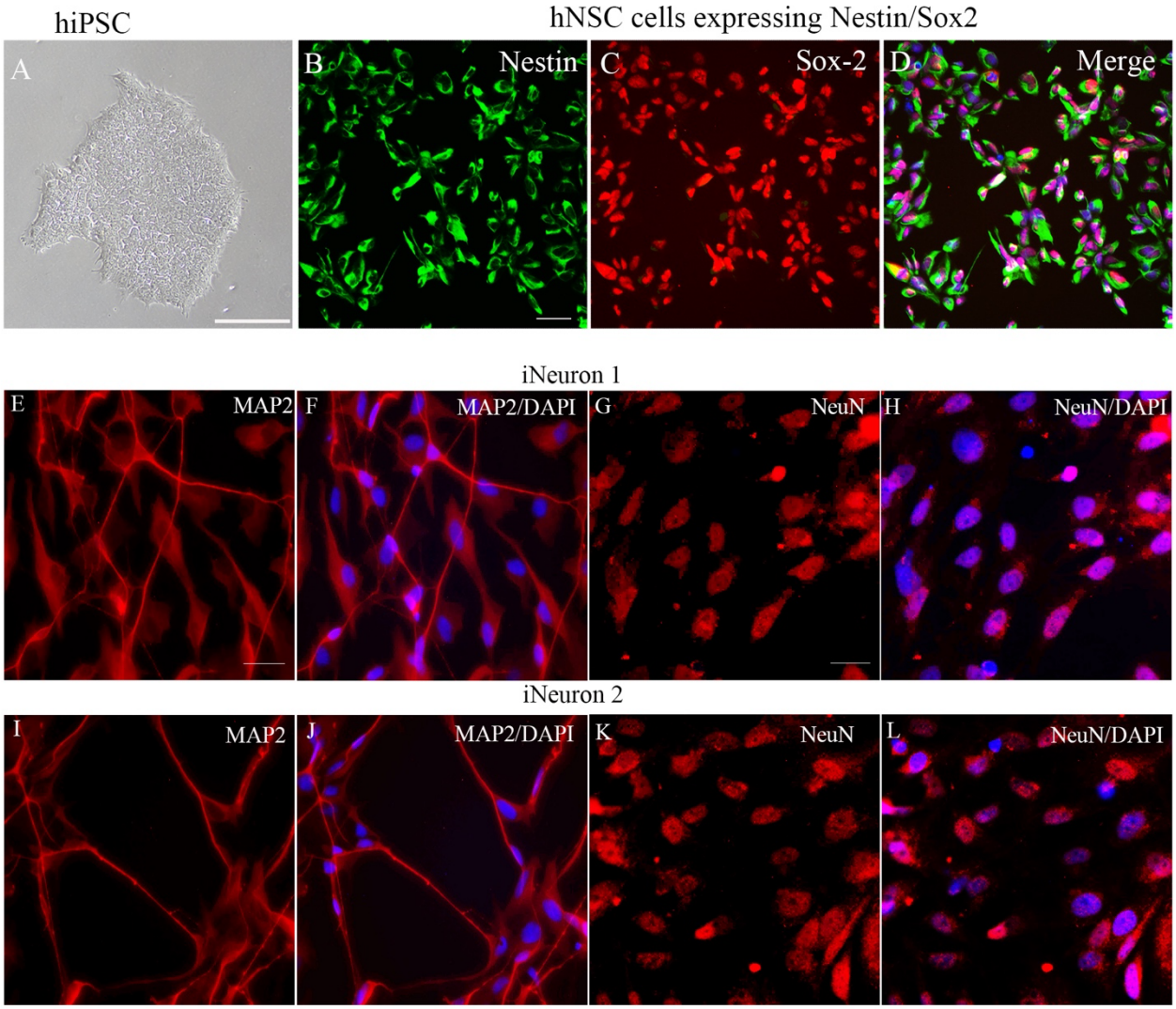

Figure 1: Generation and characterization of human neural stem cells (NSCs) and human neurons from human induced pluripotent stem cells (hiPSCs). Figure A shows a hiPSC colony. Images B-D show the expression of nestin (B), Sox-2 (C), and both nestin and Sox-2 counterstained with DAPI (D) in NSCs derived from hiPSCs. Figures E-H and I-J respectively illustrate mature neurons derived hiPSC lines 1 and 2 (iNeurons 1 and 2) immunostained with microtubule-associated protein-2 (MAP-2; E-F, I-J) and neuron-specific nuclear antigen (NeuN; G-H, K-L). Scale bars: 100 µm.

Figure 2

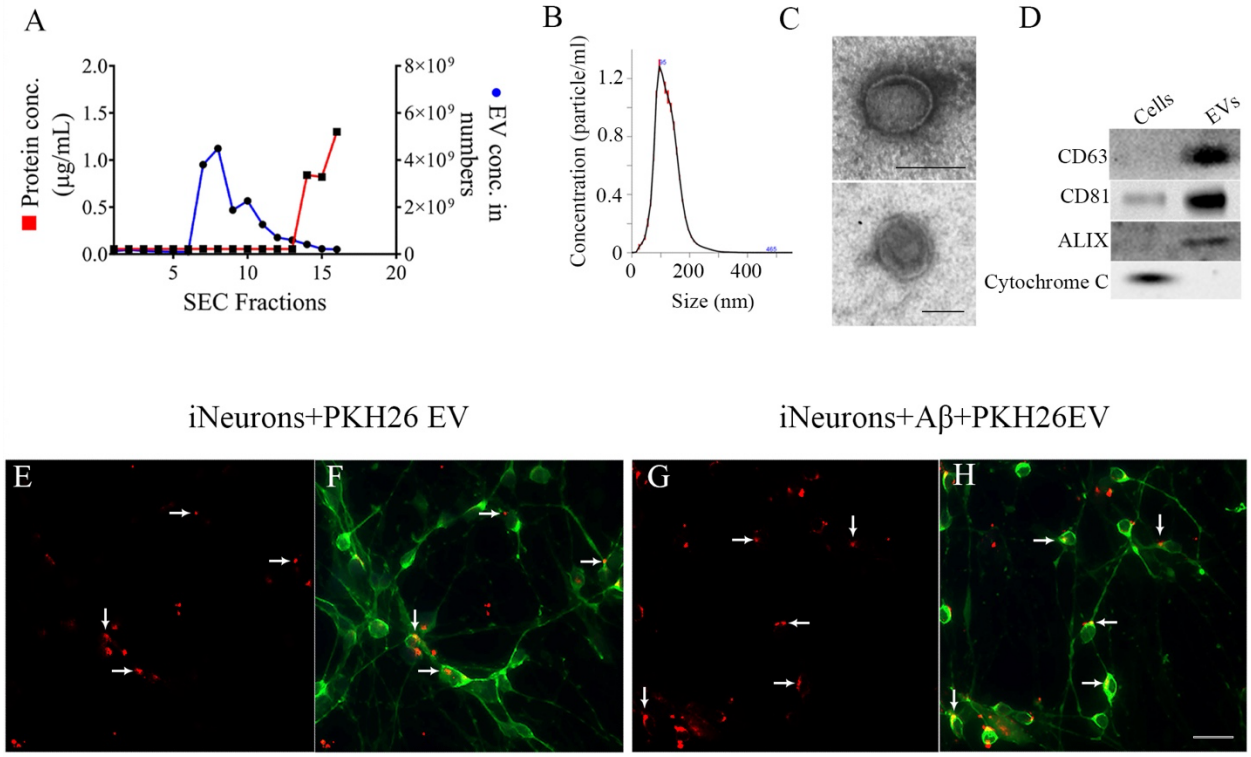

Figure 2: Characterization of extracellular vesicles from human induced pluripotent stem cell-derived neural stem cells (hiPSC-NSC-EVs). Graph A illustrates the number of EVs vis-a-vis protein content in various fractions collected from size-exclusion chromatography. Graph B shows that the average size of EVs varied between 100-200 nm, with a mean size of 121.6 nm. Figure C illustrates the morphology of EVs examined through transmission electron microscopy. Scale bar, 100 nm. Figure D shows the expression of CD63, CD81, and ALIX but not cytochrome C in hiPSC-NSC-EVs visualized through Western blotting. Full-length blots of CD63, CD81, ALIX and cytochrome C are presented in Supplementary figures 1-4. Figures E-H demonstrate the incorporation of PKH26-labeled EVs (red particles) into microtubule-associated protein-2 (MAP-2)-positive human neurons (green) in standard cultures (E-F) and Aβ-42 oligomers exposed cultures (G-H). Scale bar, 100 µm.

Figure 3

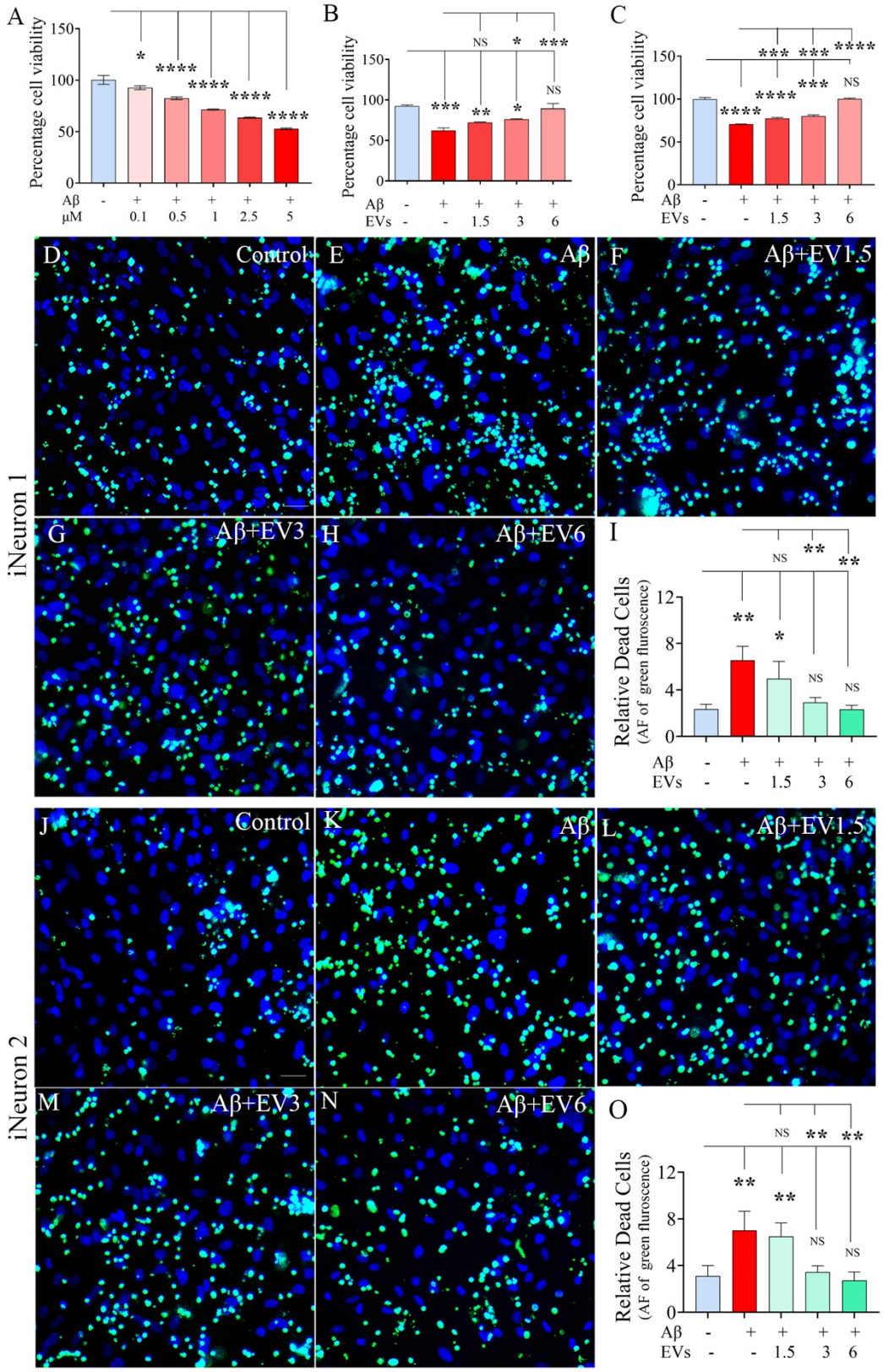
A
Percentage cell viability
150
100
50
0
Aβ - + + + + +
μM 0.1 0.5 1 2.5 5
B
Percentage cell viability
Aβ - + + + +
EVs - - 1.5 3 6
C
Percentage cell viability
Aβ - + + + +
EVs - - 1.5 3 6
D Control
E Aβ
F Aβ+EV1.5
iNeuron 1
G Aβ+EV3
H Aβ+EV6
I
Relative Dead Cells
(AF of green fluroscence)
Aβ - + + + +
EVs - - 1.5 3 6
J Control
K Aβ
L Aβ+EV1.5
iNeuron 2
M Aβ+EV3
N Aβ+EV6
O
Relative Dead Cells
(AF of green fluroscence)
Aβ - + + + +
EVs - - 1.5 3 6

Figure 3: Assessment of cell viability in iNeurons cultures exposed to Aβ-42 oligomers (Aβ-42o), or Aβ-42o and extracellular vesicles from human induced pluripotent stem cell-derived neural stem cells (hiPSC-NSC-EVs). The bar chart in A shows the results of an MTT assay comparing the percentages of viable neurons in iNeurons cultures exposed to different concentrations of Aβ-42o. The bar charts B-C show the results of MTT assays comparing the percentages of viable neurons in iNeurons 1 and 2 cultures exposed to Aβ-42o or Aβ-42o and different concentrations of hiPSC-NSC-EVs. Figures D-H and J-N are representative images from cultures of iNeurons 1 (D-H) and iNeurons 2 (J-N), processed for live and dead cell assay. D and J, control iNeurons 1 and 2 cultures. E and K, iNeurons 1 and 2 cultures exposed to Aβ-42o. F and L, iNeurons 1 and 2 cultures exposed to Aβ-42o and treated with 1.5×10^9 billion EVs. G and M, iNeurons 1 and 2 cultures exposed to Aβ-42o and treated with 3.0×10^9 billion EVs. H and N, iNeurons 1 and 2 cultures exposed to Aβ-42o and treated with 6.0×10^9 billion EVs. The bar charts I and O compare the area fractions of green fluorescence (implying dead cells) across different groups for iNeurons 1 (I) and iNeurons 2 (O) cultures; Scale bar, 100 µm.

Figure 4

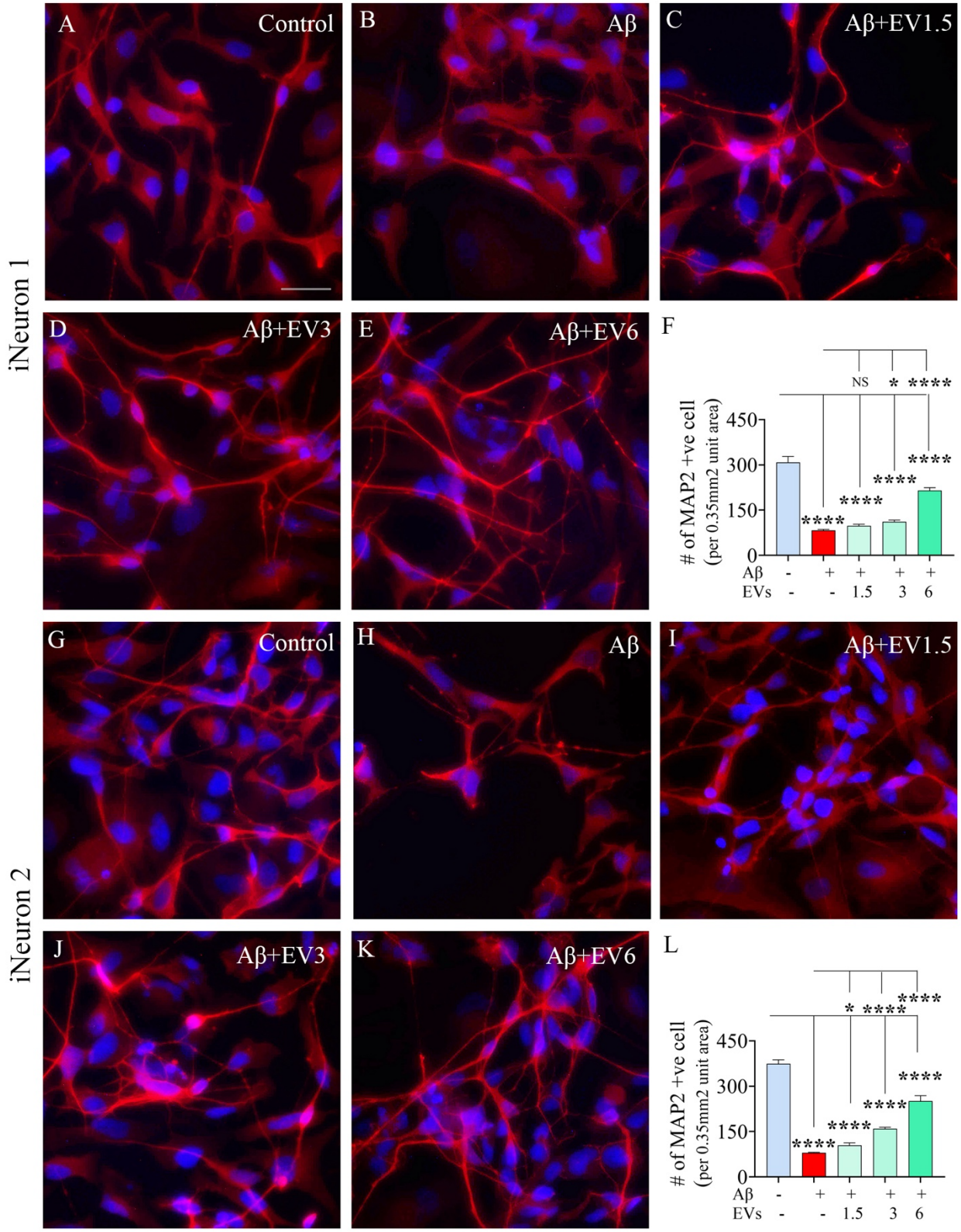
iNeuron 1
A
Control
B
Aβ
C
Aβ+EV1.5
D
Aβ+EV3
E
Aβ+EV6
F
NS
*
****
# of MAP2 +ve cell
(per 0.35mm2 unit area)
450
300
150
0
Aβ - + + + +
EVs - - 1.5 3 6
iNeuron 2
G
Control
H
Aβ
I
Aβ+EV1.5
J
Aβ+EV3
K
Aβ+EV6
L
# of MAP2 +ve cell
(per 0.35mm2 unit area)
450
300
150
0
Aβ - + + + +
EVs - - 1.5 3 6

Figure 4: The effects of adding extracellular vesicles from human induced pluripotent stem cell-derived neural stem cells (hiPSC-NSC-EVs) into iNeurons cultures on Aβ-42 oligomers (Aβ-42o)-induced neurodegeneration. Figures A-E and H-L show representative images of surviving microtubule-associated protein-2 (MAP-2) positive neurons from control cultures of iNeurons 1 and 2 (A, G), and iNeurons 1 and 2 cultures exposed to Aβ-42o alone (B, H), Aβ-42o and treated with 1.5 x 10^9 billion EVs (C, I), Aβ-42o and treated with 3.0 x 10^9 billion EVs (D, J), or Aβ-42o and treated with 6.0 x 10^9 billion EVs (E, K). Scale bar, 100 µm. The bar charts in F and L compare the numbers of surviving MAP-2+ neurons per unit area (0.35mm^2) of iNeurons 1 and iNeurons 2 cultures across various groups.

Figure 5

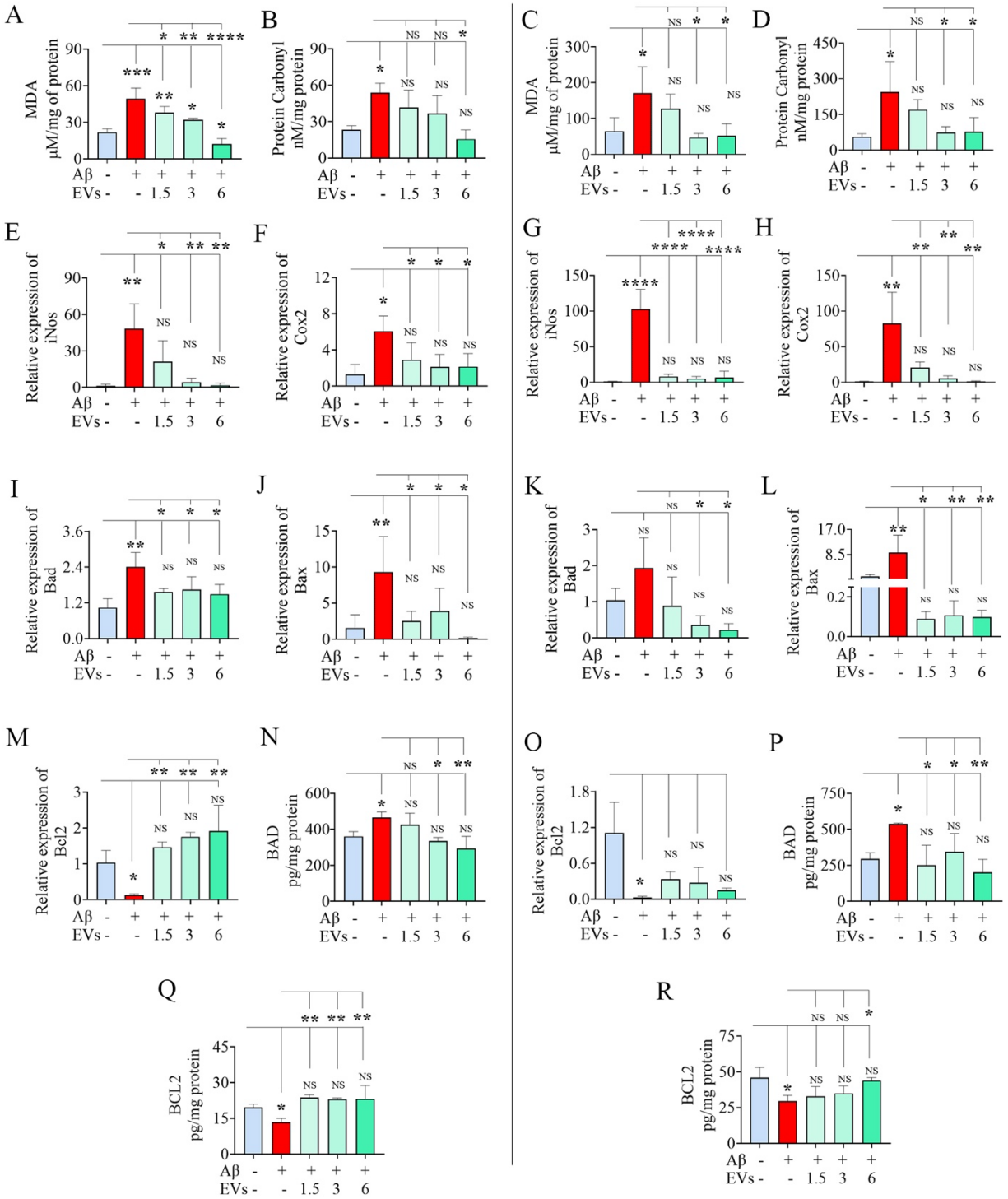

Figure 5: The effects of adding extracellular vesicles from human induced pluripotent stem cell-derived neural stem cells (hiPSC-NSC-EVs) into iNeurons cultures on Aβ-42 oligomers (Aβ-42o)-

induced oxidative stress and pro-apoptotic gene and protein expression. The bar charts A-D compare the concentrations of malondialdehyde (MDA, A, C) and protein carbonyls (B, D) in Aβ-42o exposed cultures of iNeuron 1 (A-B) and iNeuron 2 (C-D) treated with different concentrations of hiPSC-NSC-EVs. The bar charts E-H compare the relative gene expression of iNos (E, G) and Cox2 (F, H) in Aβ-42o exposed cultures of iNeurons 1 (E-F) and iNeurons 2 (G-H) treated with different concentrations of hiPSC-NSC-EVs. The bar charts I-M and O compare the relative gene expression of Bad (I, K), Bax (J, L), and Bcl2 (M, O) in Aβ-42o exposed cultures of iNeurons 1 (I-J and M) and iNeurons 2 (K-L and O) treated with different concentrations of hiPSC-NSC-EVs. The bar charts N, Q, P, and R compare the protein concentrations of BAD (N, P) and BCL2 (Q, R) in Aβ-42o exposed cultures of iNeurons 1 (N, Q) and iNeurons 2 (P, R) treated with different concentrations of hiPSC-NSC-EVs.

Figure 6

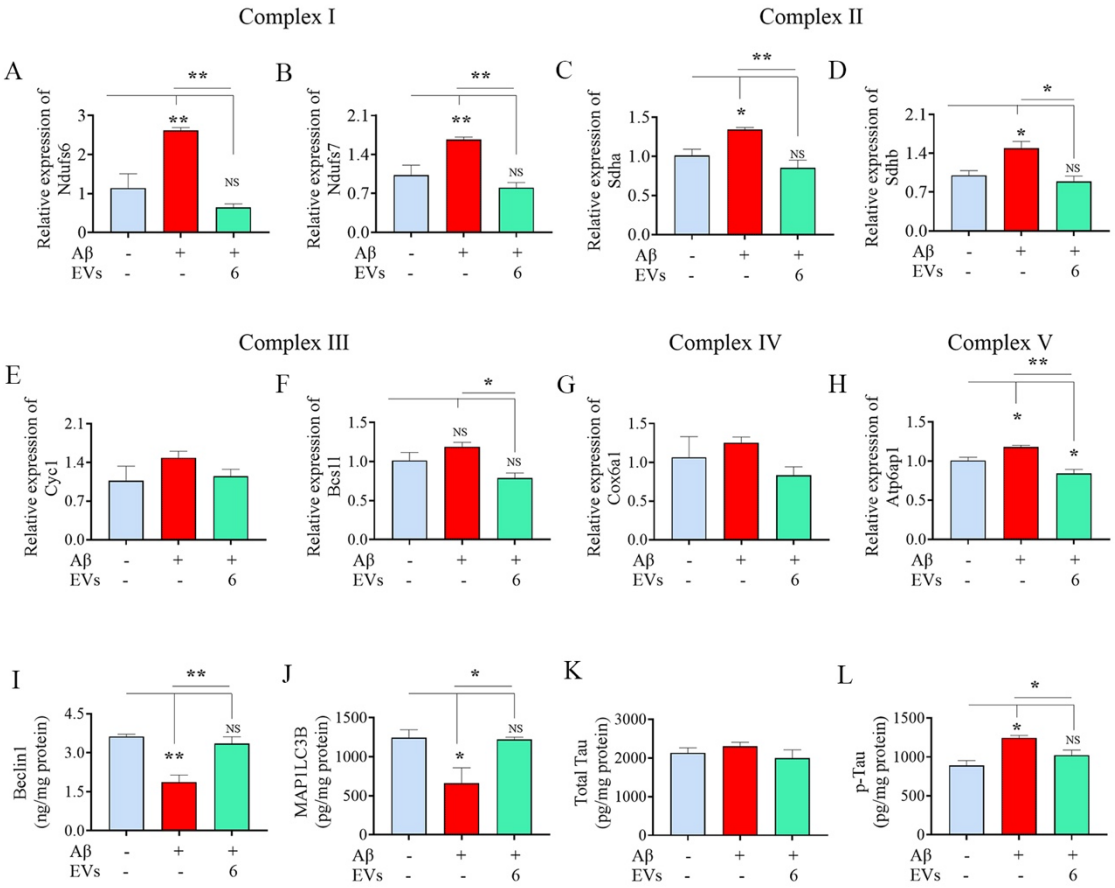

Figure 6: The effects of adding extracellular vesicles from human induced pluripotent stem cell-derived neural stem cells (hiPSC-NSC-EVs) into iNeurons cultures on Aβ-42 oligomers (Aβ-42o)-induced increase in the expression of genes encoding mitochondrial complex proteins, decrease in autophagy-related proteins and tau phosphorylation. The bar charts A-H compare the relative expression of genes Ndufs6 (A), Ndufs7 (B), Sdha (C), Sdhb (D), Cyc1 (E), Bcs1l (F), Cox6a1 (G) and Atp6ap1 (H) in Aβ-42o exposed cultures of iNeurons 1 treated with 6 x 10^9 hiPSC-NSC-EVs. The bar charts I and J compare the concentrations autophagy-related proteins Beclin 1 (I) and MAP1LC3B (J) in Aβ-42o exposed cultures of iNeurons 1 treated with 6 x 10^9 hiPSC-NSC-EVs. The bar charts K and L compare the concentrations of total tau (K) and phosphorylated-tau (p-tau, L) in Aβ-42o exposed cultures of iNeurons 1 treated with 6 x 10^9 hiPSC-NSC-EVs.